Co-published by
Institute of Fluid-Flow Machinery
Polish Academy of Sciences
Committee on Thermodynamics and Combustion
Polish Academy of Sciences

http://www.imp.gda.pl/archives-of-thermodynamics/

Numerical Analysis of Heat Transfer of CuO-Water Nanofluid Through a Square Channel with Heated Inner Triangular Groove

Baradi Lavanya[a,b], Gosukonda Srinivas[c], Baluguri Suresh Babu[d*], Oluvole Daniel Makinde[e]

[a]Bharatiya Engineering Science & Technology Innovation University, Gorantla, Andhra Pradesh- 515231, India.
[b]St. Francis College for Women, Hyderabad,Telangana-500 016, India.
[c]Geethanjali college of Engineering and Technology, Hyderabad,Telangana-500 016, India.
[d]Sreyas Institute of Engineering and Technology, Hyderabad,Telangana-500 068, India.
[e]Stellenbosch University, Private Bag X2, Saldanha 7395, South Africa.
*Corresponding author email: bsureshmaths@gmail.com.

Received: 14.08.2024; revised: 14.12.2024; accepted: 16.12.2024

Abstract

This paper investigates the flow and heat transfer characteristics of CuO–water nanofluid in a square channel with an inner triangular groove that is continuously heated. By applying a transverse magnetic field, the governing coupled and nonlinear equations are solved using the Galerkin finite element method across various Reynolds numbers. The analysis provides comprehensive insights into the effects of different parameters through stream plots and contour plots. The heat transfer rate, represented by the Nusselt number (Nu), is graphically presented for the heated inner triangular groove and thoroughly discussed. Results indicate that the flow rate significantly influences heat transfer, particularly for high Reynolds numbers, with notable effects observed in both the upper and lower parts of the channel. Optimal heat transfer is achieved at a 3% concentration of CuO nano-particles, highlighting the potential for enhanced thermal performance in such configurations.

Keywords: Heat transfer; CuO-water nanofluid; Square channel; Inner triangular groove; Finite element method

Vol. 46(2025), No. 1, 83–96; doi: 10.24425/ather.2025.154183

Cite this manuscript as: Lavanya, B., Srinivas, G., Suresh Babu, B., & Makinde, O.D. (2025). Numerical Analysis of Heat Transfer of CuO-Water Nanofluid Through a Square Channel with Heated Inner Triangular Groove. *Archives of Thermodynamics*, 46(1), 83−96.

1. Introduction

Heating systems have always been extensively studied across various fields. Researchers have continually sought to enhance the heat transfer rate and efficiency of heating systems through a variety of techniques, both experimentally and numerically, using active and passive methods. Energy exchange occurs when two systems with different temperatures come into contact, although there can also be a temperature differential within a single system. Heat transfer is the process that facilitates the transport of energy. With advancements in microelectronics and micro-manufacturing technologies, higher performance and integration of electronic devices are now achievable. This has raised concerns among heat transfer researchers due to the thermal management challenges that come with increased performance and integration.

Heat transfer, although not directly measurable or observable, can be inferred through its effects. It involves the movement of energy due to a temperature difference between solid, liquid, or gaseous objects. The study of heat transfer encompasses the production, use, conversion and exchange of thermal energy across physical systems within the field of thermal engineering.

CuO-water nanofluid has many applications in industries. The literature contains numerous research works. In particular, Karami et al. [1] did a computer simulation of turbulent flow convection in a cylinder with rectangular grooves. He looked at

Nomenclature

B_0 – constant applied magnetic field, A/m
C_p – specific heat, J/(kg K)
g – gravitational acceleration, m/s^2
Gr – Grashoff number
k – thermal conductivity, W/(m K)
L – characteristic length, m
M – magnetic field parameter
Pr – Prandtl number
q – heat source parameter, W/m^2
Q_h – dimensionless heat source parameter
Re – Reynolds number
t – dimensional time, s
T – dimensional temperature, K
T_0 – temperature at triangular groove, K
T_∞ – temperature at upper plate of the channel, K
u, v – dimensional velocity, m/s
U, V – dimensionless velocities
U_0 – characteristic velocity, m/s
x, y – dimensional space variables, m
X, Y – dimensionless space variables
$Ø$ – volume fraction of the nanoparticles

Greek Symbols

α – thermal diffusivity, m^2/s
β_T – coefficient of thermal expansion, 1/K
Θ – dimensionless temperature
μ – dynamic viscosity, Pa·s
ρ – density, kg/m^3
σ – electrical conductivity, S/m
φ_j – shape function at j^{th} node

Subscripts and Superscripts

f – base fluid (water)
nf – nanofluid (CuO-water)
s – metal particle (CuO)

Abbreviations and Acronyms

FEM – finite element method

how CuO nanoparticles at different volume fractions affect heat transfer for different Reynolds numbers. Dehghani-Ashkezari and Salimpour [2] studied how water-titanium oxide nanofluid boiled in pools on different grooved surfaces and found that the shape of the grooves has a big effect on how heat moves through the surface. In their study, Boukerma and Kadja [3] looked at the convective heat transfer of Al_2O_3/water-ethylene glycol (EG) and CuO/(W-EG) nanofluids in a round tube with laminar flow. According to Jafarimoghaddam and Aberoumand [4], nanofluids improve the flow properties in rib-groove channels, with the Nusselt number going up as the volume fraction goes up and down as the nanoparticle diameter goes down. Srinivas et al. [5] studied the natural chemical reaction between the metal particle and the solvent, along with the decomposition of the metal particle. Researchers also examined the behaviour of the nanofluid viscosity in relation to its flow and heat transfer. Gupta et al. [6] explored how to resolve the unsteady flow problem of a hybrid nanofluid on a stretched surface in a porous medium. This study examines the form factor analysis by evaluating four geometries: brick, lamina, platelet and blade.

The experiments of heat and mass transfer through many geometries, like horizontal and vertical channels, are available in the literature. Balasubramanian and Mukeshkumar [7] conducted additional research and determined that the size of the nanoparticles and their thermal conductivity significantly influence the efficacy of heat transfer. Navaei et al. [8] investigated the impact of various nanofluids and geometrical parameters on rib-grooved channels. They discovered that the heat transfer properties varied based on the basal fluids. Rimbault et al. [9] noted that nanofluids exhibit minor improvements in heat transfer compared to water due to their low particle volume fractions. Ahmed et al. [10] used a turbulence model to look into the turbulent forced convection of nanofluids in channels that are triangularly corrugated and have different Reynolds numbers. The objective was to emphasize the impact of rib dimensions on heat transfer.

The finite element method (FEM) has become a crucial computational tool in engineering and applied sciences, solving complex problems in structural, thermal, fluid, and electromagnetic domains. FEM applications span various fields, including mechanical engineering, civil engineering, bioengineering, and materials science, providing accurate simulations of heat flow in systems with intricate shapes and varying thermal properties. Ekiciler [11] did a test to see how new hybrid nanofluids (TiO_2-Cu/EG) and the shape of a triangular rib in a duct changed the flow and transfer of heat. They discovered that a volume fraction of 4% is necessary. Suresh Babu et al. [12] created a mathematical model that includes thermo-diffusion and diffusion-thermal effects for heat and mass transfer in a variable-width vertical channel between two fluids that don't mix. In the research by Gupta et al. [13], they look at how radiation and Thompson and Troian boundary slip affect the flow of a nanofluid that is made up of kerosene oil and CNT-Fe_3O_4 over an exponentially stretched porous sheet. The Reynolds viscosity model views the viscosity as temperature-dependent. Ahmed et al. [14] used the finite volume method to study the impact of nanofluid volume on entropy and turbulent kinetic energy. Vatani and Mohammed [15] numerically examined the effects of rib groove shapes and nanofluids on heat and fluid flow in horizontal channels.

Also, FEM has a lot of advantages; it can handle complex geometries like a square channel with different shapes of grooves. FEM is well-suited for problems with boundary and interface complexities. Ajeel et al. [16], Alipour et al. [17], Hussein et al. [18], and Naphon and Nakharintr [19] conducted a study that explored various nanofluid configurations and their effects on turbulent flow and heat transfer. Gosty et al. [20] examine the phenomena of heat, mass, and fluid flow in a vertical channel holding two immiscible fluids, with an emphasis on slip effects. Upreti et al. [21] analyze Au-TiO_2/ethylene glycol hybrid nanofluid flow across a narrow needle. In a homogeneous magnetic field, fluid parameters like dynamic viscosity and thermal conductivity rely on nanoparticle shape and temperature. They also examine quadratic convection with quadratic thermal

radiation and use the Cattaneo-Christov heat flow model to explain heat transfer. Some researchers, like Avramenko et al. [22] and Ajeel et al. [23] looked into the thermal and hydraulic properties of turbulent nanofluid flow. Other researchers, like Khudheyer et al. [24] and Pourfattah et al. [25] looked into how nanoparticles and rib angles affect heat transfer. Sailaja et al. [26] conducted research on forced and free convective heat transfer through a two-dimensional nanofluid flowing past a stretching vertical plate. In a study by Akdag et al. [27] they measured how heat moved through water-based Al_2O_3 nanofluids in a wavy mini-channel. They found that the size and number of nanoparticles had a big effect on how well the heat moved. Uniyal et al. [28] examined it in depth. They conducted a thorough investigation into the integration of phase change materials and nanofluids into evacuated tube solar water heaters, an area that has witnessed significant advancements recently. Gosty et al. [29] conducted a study that explores the transmission of heat and mass in a vertical channel filled with immiscible fluids, specifically viscous and micropolar fluids. Bhandari et al. [30] looked into modifying the design of the microchannel heat sink to enhance thermo-hydraulic performance.

The aforementioned research reveals that while traditional studies concentrate on straightforward flow patterns, this study delves into the distinctive impact of the triangular groove, amplifying the heat transfer effects. So the primary objective of this work is to investigate the flow and heat transfer characteristics of CuO-water nanofluid through a square channel with a heated inner triangular groove. The groove geometry disturbs the flow, and the induced temperature due to the geometry plays a vital role in heat transfer analysis. This study aims to help improve the thermal management of advanced cooling systems in high-performance settings by using CuO nanoparticles, which are known for being excellent at transferring heat, and look at how they change heat transfer under different flow conditions. Detailed computational simulations provide a deeper understanding of the intricate heat transfer phenomena in advanced engineering applications such as solar water heaters and industrial heat exchangers.

2. Mathematical Formulation

To mathematically formulate the flow and heat transfer of a fully developed nanofluid in a square pipe with an isosceles triangular groove at the bottom, the following assumptions need to be considered:

- Flow direction: The nanofluid flows in the *z*-axis direction.
- Cross-sectional geometry: The cross-section is square with an isosceles triangular groove at the bottom.
- Boundary conditions: Vertical walls: Adiabatic.
- Top wall: Constant temperature T_∞.
- Inclined triangular walls: Constant temperature T_0.
- Bottom wall: Adiabatic (excluding the triangle).
- $T_0 > T_\infty$.

The typical cross section as shown in Fig. 1, is assumed for the numerical study.

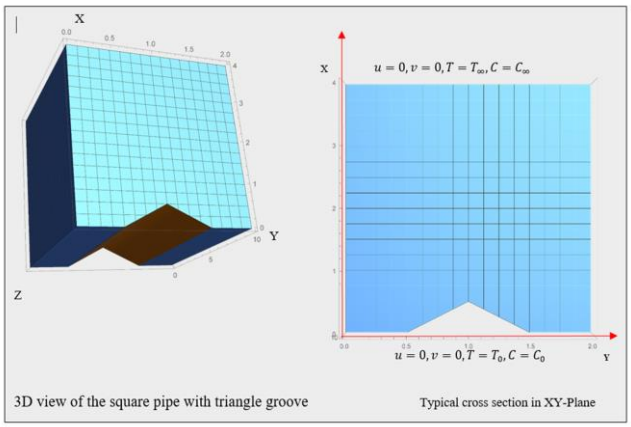

Fig. 1. Geometry of the problem

Under these assumptions, the flow system is assumed to follow the Bussinesq approximation and as per the Buongiorno model, the equations governing the flow, heat and mass transfer are obtained as follows:

$$\frac{\partial u}{\partial x} + \frac{\partial v}{\partial y} = 0, \tag{1}$$

$$\rho_{nf}\left(\frac{\partial u}{\partial t} + u\frac{\partial u}{\partial x} + v\frac{\partial u}{\partial y}\right) = \mu_{nf}\left(\frac{\partial^2 u}{\partial x^2} + \frac{\partial^2 u}{\partial y^2}\right) + \\ +(\rho\beta_T)_{nf} g(T - T_\infty) - \sigma_{nf} {B_0}^2 u, \tag{2}$$

$$\rho_{nf}\left(\frac{\partial v}{\partial t} + u\frac{\partial v}{\partial x} + v\frac{\partial v}{\partial y}\right) = \mu_{nf}\left(\frac{\partial^2 v}{\partial x^2} + \frac{\partial^2 v}{\partial y^2}\right), \tag{3}$$

$$\frac{\partial T}{\partial t} + u\frac{\partial T}{\partial x} + v\frac{\partial T}{\partial y} = \alpha_{nf}\left(\frac{\partial^2 T}{\partial x^2} + \frac{\partial^2 T}{\partial y^2}\right) - \frac{Q}{(\rho C_p)_{nf}}. \tag{4}$$

The boundary conditions are:
at $t \geq 0$, at the inner triangular groove

$$u = 0, \quad v = 0, \quad T = T_0, \tag{5a}$$

at $t \geq 0$, $y = L$, $\forall x$

$$u = 0, \quad v = 0, \quad T = T_\infty. \tag{5b}$$

All the above equations are made dimensionless using the following forms:

$$X = \frac{x}{L}, \quad Y = \frac{y}{L}, \quad t' = t\frac{U_0}{L}, \\ U = \frac{u}{U_0}, \quad V = \frac{v}{U_0}, \quad \theta = \frac{T - T_\infty}{T_0 - T_\infty}, \tag{6}$$

where L is the characteristic length and U_0 is the characteristic velocity.

Thermophysical properties considered for this CuO water nanofluid are taken from the work of Pak and Cho [31].

$$\rho_{nf} = (1 - \emptyset)\rho_f + \emptyset\rho_s, \tag{7}$$

$$(\rho C_p)_{nf} = (1 - \emptyset)\left(\rho C_p\right)_f + \emptyset(\rho C_p)_s, \tag{8}$$

$$\frac{k_{nf}}{k_f} = \frac{k_s + 2k_f + 2\emptyset\,(k_s - k_f)}{k_s + 2k_f - \emptyset\,(k_s - k_f)}, \tag{9}$$

$$(\rho\beta)_{nf} = (1-\emptyset)(\rho\beta)_f + \emptyset(\rho\beta)_s, \tag{10}$$

$$\alpha_{nf} = \frac{k_{nf}}{(\rho C_p)_{nf}}, \tag{11}$$

$$\frac{\mu_{nf}}{\mu_f} = \frac{1}{(1-\emptyset)^{2.5}}, \tag{12}$$

$$\frac{\sigma_{nf}}{\sigma_f} = 1 + \frac{3\left(\frac{\sigma_s}{\sigma_f}-1\right)\emptyset}{\left(\frac{\sigma_s}{\sigma_f}+2\right)-\left(\frac{\sigma_s}{\sigma_f}-1\right)\emptyset}. \tag{13}$$

Values of thermophysical properties given in Table 1 are considered to get the numerical solution.

Table 1. Values of thermophysical properties.

Physical properties	Copper (CuO)	Water
C_p, J/(kg·K)	385	4,179
ρ, kg/m³	8,933	997.1
k, W/(m·K)	401	0.613
β_T x 10⁻⁵, 1/K	1.67	27.6
μ, kg/(m·s)	-	8.55 x 10⁻⁴
σ, S/m	0.064	0.05

In view of Eqs. (5) to (13), the governing Eqs. (1) to (4) are modified as follows:

$$\frac{\partial U}{\partial t} + U\frac{\partial U}{\partial X} + V\frac{\partial U}{\partial Y} = \frac{\frac{1}{(1-\emptyset)^{2.5}}}{1-\emptyset+\emptyset\left(\frac{\rho_S}{\rho_f}\right)}\frac{1}{\mathrm{Re}}\left(\frac{\partial^2 U}{\partial X^2}+\frac{\partial^2 U}{\partial Y^2}\right) +$$

$$+\left(1-\emptyset+\emptyset\left(\frac{\beta_s}{\beta_f}\right)\right)\frac{\mathrm{Gr}}{\mathrm{Re}^2}(\theta) - \left(1+\frac{3\left(\frac{\sigma_s}{\sigma_f}-1\right)\emptyset}{\left(\frac{\sigma_s}{\sigma_f}+2\right)-\left(\frac{\sigma_s}{\sigma_f}-1\right)\emptyset}\right) M\,U, \tag{14}$$

$$\frac{\partial V}{\partial t} + U\frac{\partial V}{\partial X} + V\frac{\partial V}{\partial Y} = \frac{\frac{1}{(1-\emptyset)^{2.5}}}{1-\emptyset+\emptyset\left(\frac{\rho_S}{\rho_f}\right)}\frac{1}{\mathrm{Re}}\left(\frac{\partial^2 V}{\partial X^2}+\frac{\partial^2 V}{\partial Y^2}\right), \tag{15}$$

$$\frac{\partial \Theta}{\partial t} + U\frac{\partial \Theta}{\partial X} + V\frac{\partial \Theta}{\partial Y} = \frac{\frac{k_S+2k_f+2\emptyset\,(k_S-k_f)}{k_S+2k_f-\emptyset\,(k_S-k_f)}}{1-\emptyset+\emptyset\left(\frac{(\rho c_p)_s}{(\rho c_p)_f}\right)}\frac{1}{\mathrm{Pr}}\frac{1}{\mathrm{Re}}\left(\frac{\partial^2 U}{\partial X^2}+\frac{\partial^2 U}{\partial Y^2}\right) +$$

$$-\frac{Q_h}{1-\emptyset+\emptyset\left(\frac{(\rho c_p)_s}{(\rho c_p)_f}\right)}\frac{1}{\mathrm{Pr}}\frac{1}{\mathrm{Re}}. \tag{16}$$

where the dimensionless numbers are given as follows:

$$\mathrm{Gr} = \frac{g\beta_T(T_\infty - T_0)L^3}{{\nu_f}^2}, \qquad \mathrm{Pr} = \frac{\nu_f}{\alpha_f}, \qquad M = \frac{\sigma_f {B_0}^2}{\rho_f L},$$
$$\mathrm{Ar} = \frac{\mathrm{Gr}}{\mathrm{Re}^2}, \qquad \mathrm{Re} = \frac{LU_0}{\nu}. \tag{17}$$

After applying the forms given in Eq. (6) the boundary conditions given in Eqs. (5a) and (5b) becomes as below:
at $t \geq 0$, at the inner triangular groove

$$U = 0, \qquad V = 0, \qquad \theta = 1, \tag{18a}$$

at $t \geq 0$, on the upper plate

$$U = 0, \qquad V = 0, \qquad \theta = 0. \tag{18b}$$

The rate of heat transfer (Nusselt number) at the inner triangular groove is calculated using the formula:

$$\mathrm{Nu} = -\frac{k_{nf}}{k_f}\left\{\int_A^B \frac{\partial\theta}{\partial X}dY + \int_B^C \frac{\partial\theta}{\partial X}dY\right\}. \tag{19}$$

3. Method of solution

The coupled nonlinear system of partial differential equations governing the flow and heat transfer, as described in Eqs. (14) to (16), is solved subject to the boundary conditions specified in Eq. (18). The Galerkin finite element method (FEM) is employed to solve this system as per the flow chart given in Fig. 2.

Numerical calculations are carried out using the Mathematica 10.1 program, and the results are presented in the form of contour and stream graphs. Additionally, a table showing the rate of heat transmission (Nusselt number Nu) is provided. During the computations, the region is partitioned into 316 elements. The number of elements (316) is determined by testing the convergence of Nu by means of trial and error. When determining the grid size and calculating the outcomes of the governing variables for different values of a given parameter, the remaining parameters are kept constant as follows: Ø = 3%, M = 5, Q =5, Gr = 5, Pr = 6.99.

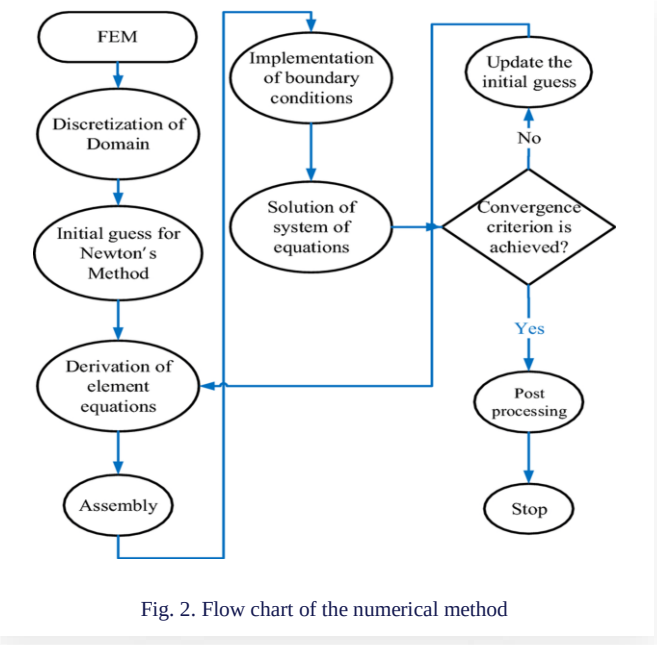

Fig. 2. Flow chart of the numerical method

This approach ensures that the FEM discretization is sufficiently refined to capture the detailed behaviour of flow, heat, and mass transfer processes within the square channel featuring a heated inner triangular groove. The convergence tests confirm the accuracy and reliability of the numerical solutions obtained.

The element wise stiffness matrix will be calculated using the following system of equations:

$$\begin{bmatrix} x_1 \\ x_2 \\ x_3 \\ x_4 \end{bmatrix} * \begin{bmatrix} u \\ v \\ \theta \\ s \end{bmatrix} = \begin{bmatrix} y_1 \\ y_2 \\ y_3 \\ y_4 \end{bmatrix}$$

where:

$$x_1 = \iint \varphi_j \left(\frac{\partial U}{\partial t} + U\frac{\partial U}{\partial X} + V\frac{\partial U}{\partial Y} - \frac{\frac{1}{(1-\emptyset)^{2.5}}}{\left(1-\emptyset+\emptyset\left(\frac{\rho_s}{\rho_f}\right)\right)}\frac{1}{\mathrm{Re}}\left(\frac{\partial^2 U}{\partial X^2} + \frac{\partial^2 U}{\partial Y^2}\right) + \right.$$
$$\left. + \left(1 - \emptyset + \emptyset\left(\frac{\sigma_s}{\sigma_f}\right)\right) M^2 U\right) dxdy,$$

$$x_2 = \iint \varphi_j \left(\frac{\partial U}{\partial t} + U\frac{\partial U}{\partial X} + V\frac{\partial U}{\partial X} - \frac{\frac{1}{(1-\emptyset)^{2.5}}}{\left(1-\emptyset+\emptyset\left(\frac{\rho_s}{\rho_f}\right)\right)}\frac{1}{\mathrm{Re}}\left(\frac{\partial^2 U}{\partial X^2} + \frac{\partial^2 U}{\partial Y^2}\right) + \right.$$
$$\left. + \left(1 - \emptyset + \emptyset\left(\frac{\sigma_s}{\sigma_f}\right)\right) M^2 U\right) dxdy,$$

$$x_{3=} \iint \left(\varphi_j \left(\frac{\partial \theta}{\partial t} + U\frac{\partial \theta}{\partial X} + V\frac{\partial \theta}{\partial Y} - \frac{\frac{k_s+2k_f+2\emptyset\left(k_s-k_f\right)}{k_s+2k_f-\emptyset\left(k_s-k_f\right)}}{(1-\emptyset+\emptyset(\frac{(\rho C_p)_s}{(\rho C_p)_f})}\frac{1}{\mathrm{Pr}}\frac{1}{\mathrm{Re}} \times \right.\right.$$
$$\times \left(\frac{\partial^2 \theta}{\partial X^2} + \frac{\partial^2 \theta}{\partial Y^2}\right) + \frac{Q_h}{(1-\emptyset+\emptyset(\frac{(\rho C_p)_s}{(\rho C_p)_f})}\frac{1}{\mathrm{Pr}}\frac{1}{\mathrm{Re}}\theta +$$
$$\left.\left. + N_b\left(\left(\frac{\partial S}{\partial Y}\right)\left(\frac{\partial \theta}{\partial Y}\right) + \left(\frac{\partial S}{\partial X}\right)\left(\frac{\partial \theta}{\partial X}\right)\right) + N_t\left(\left(\frac{\partial \theta}{\partial X}\right)^2 + \left(\frac{\partial \theta}{\partial Y}\right)^2\right)\right) dxdy,$$

$$x_{4=} \iint \left(\varphi_j \left(\left(\frac{\partial S}{\partial t}\right) + U\left(\frac{\partial S}{\partial X}\right) + V\left(\frac{\partial S}{\partial Y}\right) - N_b L_n \left(\frac{\partial^2 S}{\partial X^2} + \frac{\partial^2 S}{\partial Y^2}\right) dxdy,\right.\right.$$

$$y_{1=} \iint \varphi_j \left[\left(1 - \emptyset + \emptyset\left(\frac{\beta_s}{\beta_f}\right)\right)\frac{\mathrm{Gr}}{\mathrm{Re}^2}\left(\theta + \frac{\mathrm{Gc}}{\mathrm{Gr}}s\right)\right] dxdy,$$

$$y_{2=} 0,$$

$$y_{3=} 0,$$

$$y_4 = N_t \iint \varphi_j \left(\frac{\partial^2 \theta}{\partial X^2} + \frac{\partial^2 \theta}{\partial Y^2}\right) dxdy,$$

where the integral is done on the domain under consideration.

Each dependent variable at every 3 nodded triangular elements of the discretized domain is taken as:

$$\sum_{j=1}^{3}\sum_{i=1}^{3} u_i\varphi_j, \qquad \sum_{j=1}^{3}\sum_{i=1}^{3} v_i\varphi_j,$$
$$\sum_{j=1}^{3}\sum_{i=1}^{3} S_i\varphi_j, \qquad \sum_{j=1}^{3}\sum_{i=1}^{3} \theta_i\varphi_j.$$

The φ_j is the shape function at j^{th} node of the triangular element. The above system of equations is solved with the given approximations. This approach ensures that the FEM discretization is sufficiently refined to capture the detailed behaviour of the flow, heat and mass transfer processes within the square channel featuring a heated inner triangular groove. The convergence tests confirm the accuracy and reliability of the numerical solutions obtained.

4. Results and discussion

The results of numerical simulations, obtained through the Galerkin finite element method (FEM) using Mathematica 10.1, provide detailed insights into the heat and mass transfer characteristics of CuO-water nanofluid in a square channel with a heated inner triangular groove. The computational domain, discretized into 316 elements, ensures a high level of accuracy, as confirmed by the convergence tests of the Nusselt number. The results are presented in the form of contour and stream plots, which visually depict the flow patterns and temperature distributions within the channel. These plots highlight the effects of the triangular groove and the presence of CuO nanoparticles on the overall heat transfer performance. Additionally, the analysis of Nu provides a quantitative measure of the heat transfer rate, allowing for a detailed discussion of the impact of various parameters on thermal efficiency. The discussion focuses on the influence of the flow rate, magnetic field, and nanoparticle concentration on the heat transfer and fluid flow characteristics. The findings for all significant variations are illustrated in stream plots from Fig. 3 to Fig. 8, providing a clear depiction of the stream field profiles. These findings are presented for three distinct flow regimes: laminar conditions at low Reynolds numbers (Re = 10), transition conditions at moderate Reynolds numbers (Re = 100), and at high Reynolds numbers (Re = 5000). The effects of varying CuO particle volume fractions and Reynolds numbers on the flow and heat transfer are analysed.

4.1. Stream plots

Figures 3–6 show that at a Reynolds number (Re) of 10, the flow pattern is distinctly laminar and smooth, indicating stable and uniform flow characteristics. However, as the Reynolds number increases to 100 and 5000, the flow transitions to more complex states, exhibiting significant changes in behaviour. For Re = 100, the flow begins undergo the transition, showing the early stages of instability and the development of non-uniformties. At Re = 5000, the flow becomes fully turbulent, characterized by chaotic and irregular patterns. In both the transitional (Re = 100) and turbulent (Re = 5000) cases, the flow is notably non-uniform across the channel, regardless of the percentage of metal particle composition. This non-uniformity is particularly pronounced around the heated triangular groove, where the recirculation zones and vortices are more prominent. Gravity influences the flow near the lower half of the channel, causing fluid accumulation and complex flow patterns around the groove. However, significant flow changes are also observed in the upper half of the channel. The presence of higher concentrations of CuO particles amplifies these effects. At higher particle concentrations, the fluid exhibits increased thermal conductivity and altered viscosity, which contribute to the more pronounced flow alterations. The CuO particles enhance the heat transfer but also lead to more complex flow interactions, especially in the upper half of the channel. This results in a distinct presence of fluid with higher particle content in this region, affecting the overall flow dynamics and heat transfer efficiency within the channel.

The magnetic field parameters play a crucial role in understanding and predicting the dynamics of magnetized fluids. The strength of the magnetic field is a fundamental parameter that directly influences the behaviour of the fluid. Higher magnetic field strengths lead to stronger interactions of CuO particles with the fluid, affecting its flow patterns, stability and transport prop-

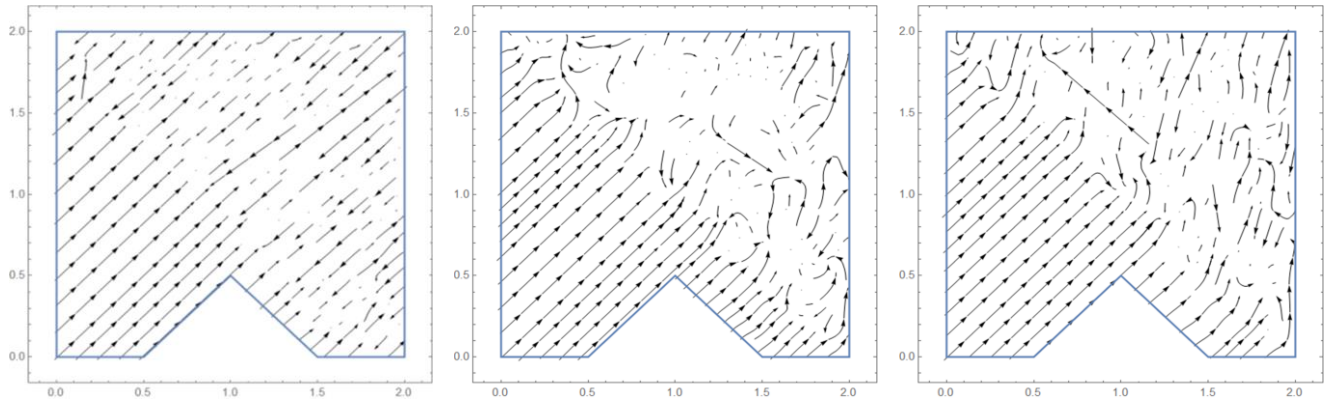

Fig. 3. Stream plots for Ø = 1% for different Reynolds numbers: Re = 10, 100 and 5000, respectively.

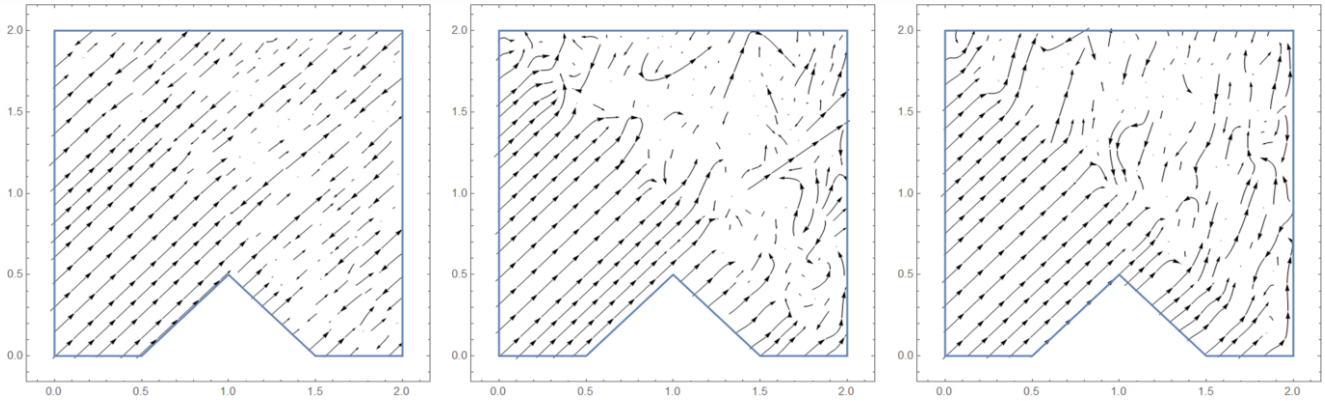

Fig. 4. Stream plots for Ø = 2% for different Reynolds numbers: Re = 10, 100 and 5000, respectively.

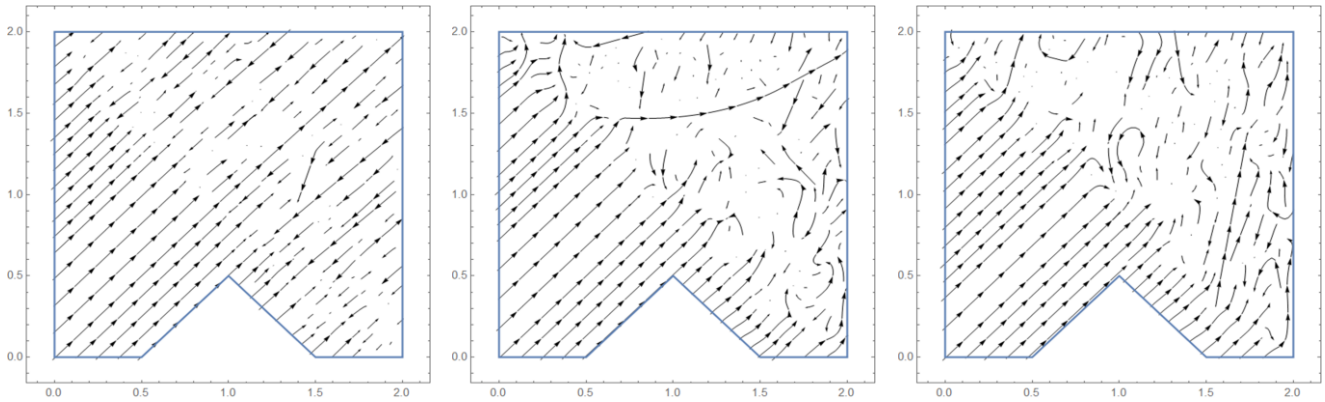

Fig. 5. Stream plots for Ø = 3% for different Reynolds numbers: Re = 10, 100, 5000 respectively.

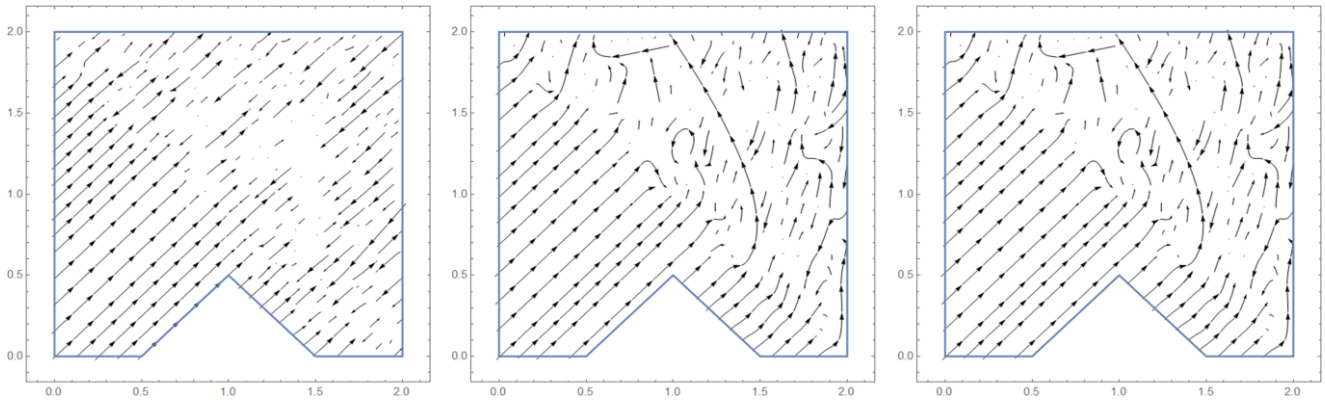

Fig. 6. Stream plots for Ø = 4% for different Reynolds numbers: Re = 10, 100 and 5000, respectively.

erties. Figures 7−10 show that there is a slight flow disturbance observed when the magnetic field parameter varies from $M = 2$ to $M = 10$ at Re = 10 (laminar flow). A uniform flow near the inner triangular groove up to $M < 8$ is noticed. But for $M > 8$, the flow behaviour changes significantly. However, lower magnetic field parameters are strongly recommended to reduce the flow turbulence to a greater extent.

Figures 11−14 illustrate the temperature distribution within the channel, highlighting the impact of the heat source on thermal gradients. The presence of the heated triangular groove introduces localized high-temperature regions, resulting in significant thermal expansion of the fluid and variations in the density of both the fluid and CuO particles. This thermal expansion causes deformation of the streamlines at the heat source, particu-

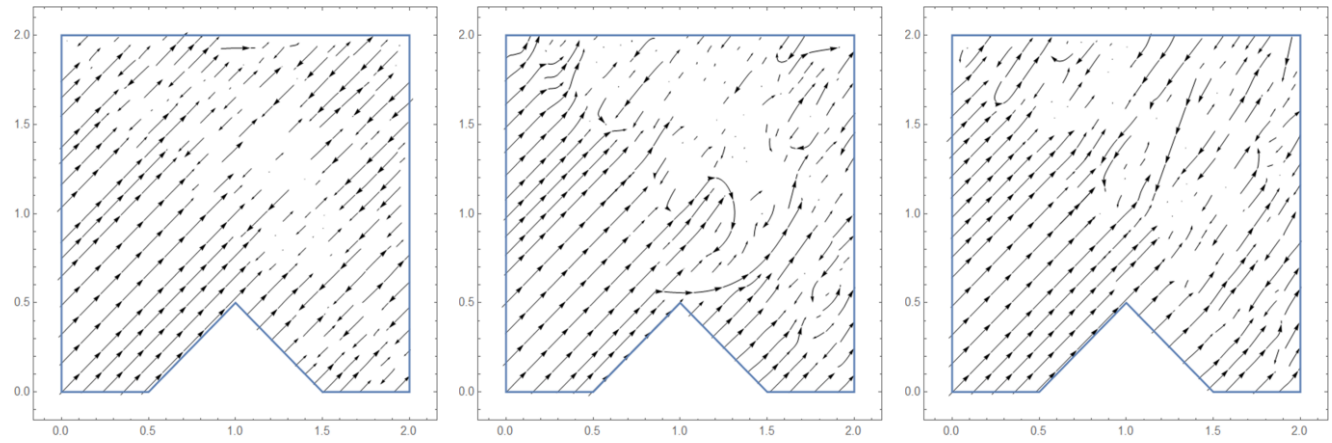

Fig. 7. Stream plots for $M = 2$ for different Reynolds numbers: Re = 10, 100 and 5000, respectively.

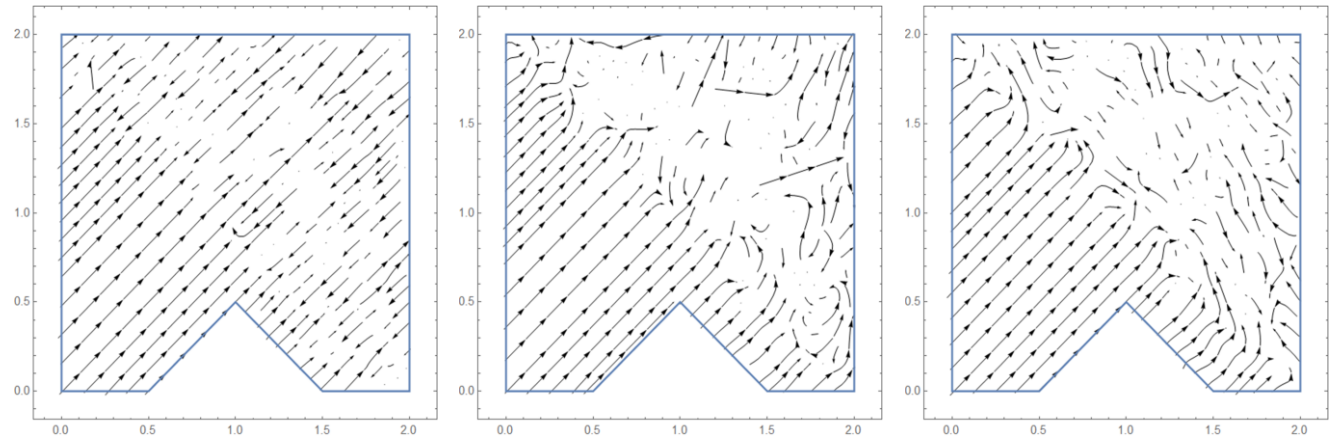

Fig. 8. Stream plots for $M = 5$ for different Reynolds numbers: Re = 10, 100 and 5000, respectively.

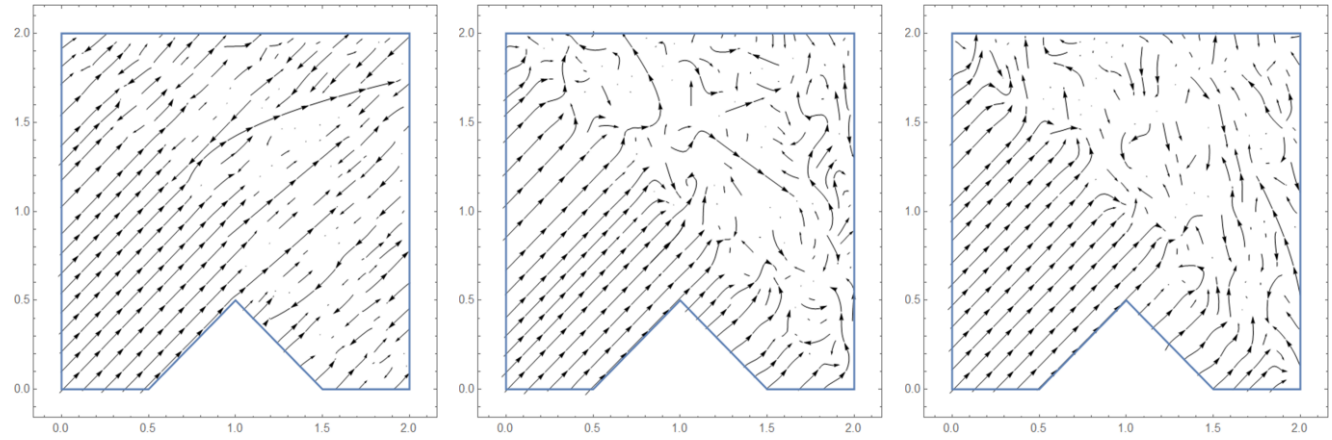

Fig. 9. Stream plots for $M = 8$ for different Reynolds numbers: Re = 10, 100 and 5000, respectively.

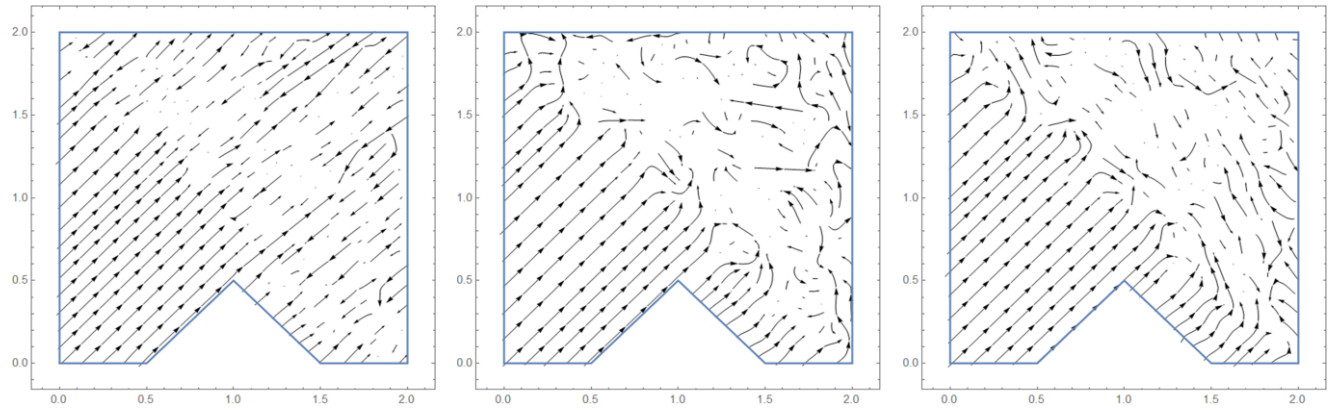

Fig. 10. Stream plots for M = 10 for different Reynolds numbers: Re = 10, 100 and 5000, respectively.

larly around the triangular groove, indicating changes in the flow pattern induced by the heat. In these regions, the streamlines exhibit noticeable curvature or deviation, corresponding to areas of convective motion where heat is being transported through the fluid. The thermal gradients create buoyancy effects, which further alter the flow pattern. This is especially evident in the upper half of the channel, where turbulence is more pronounced. The internal heat source acts as an additional factor, intensifying the disturbances in this region. The results show that the heat source significantly influences the temperature field, causing more pronounced disturbances and complex flow behaviour near the upper half of the channel. The increased turbulence and convective heat transfer lead to greater mixing and enhanced thermal diffusion, reflected in the curved and deviated streamlines. These effects underscore the crucial role of thermal gradients and heat sources in shaping the flow and temperature distribution within the channel.

4.2. Contour plots

Figures 15−18 illustrate the temperature distribution contours for various heat source values in different flow regimes. At lower values of the heat source parameter (Q) in laminar flow, the temperature is predominantly higher in the lower part of the

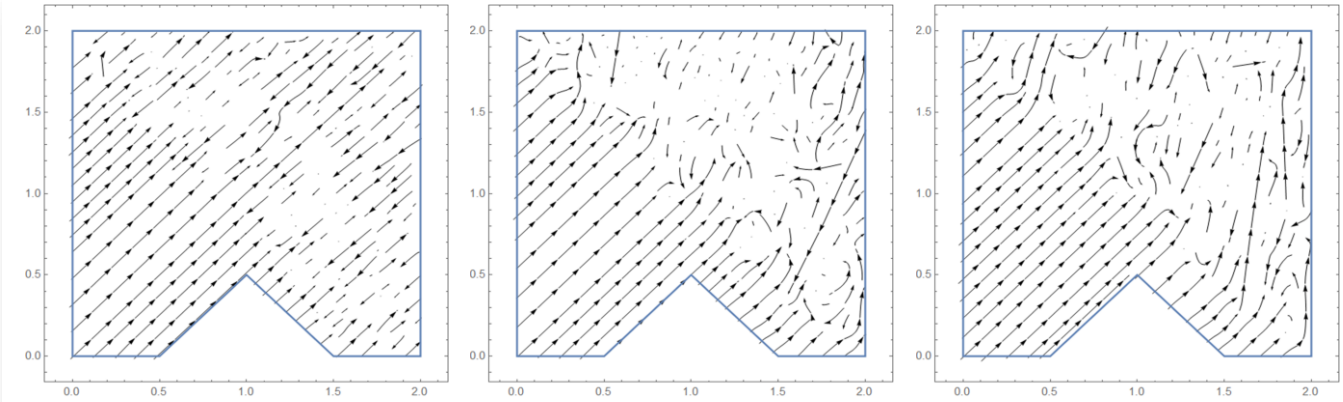

Fig. 11. Stream plots for Q = 5 for different Reynolds numbers: Re = 10, 100 and 5000, respectively.

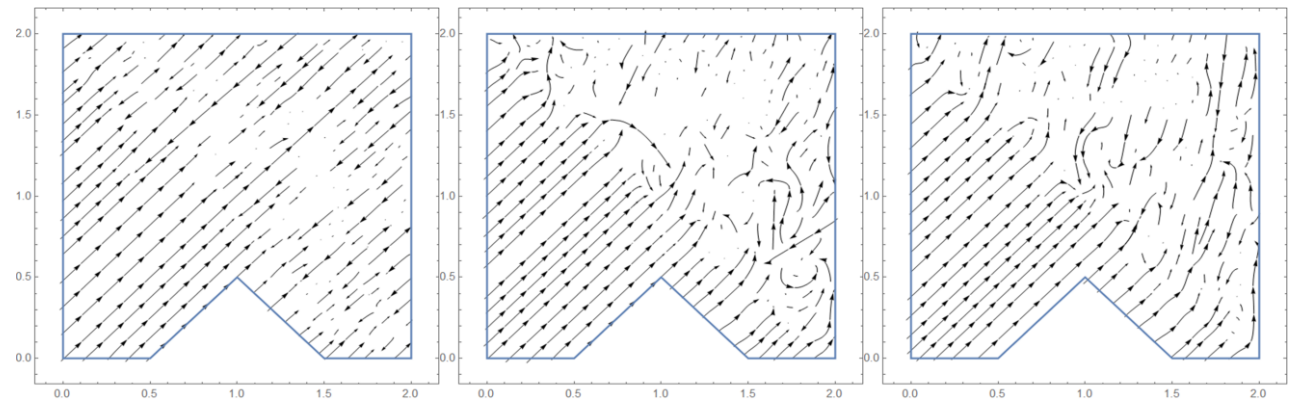

Fig. 12. Stream plots for Q = 12 for different Reynolds numbers: Re = 10, 100 and 5000, respectively.

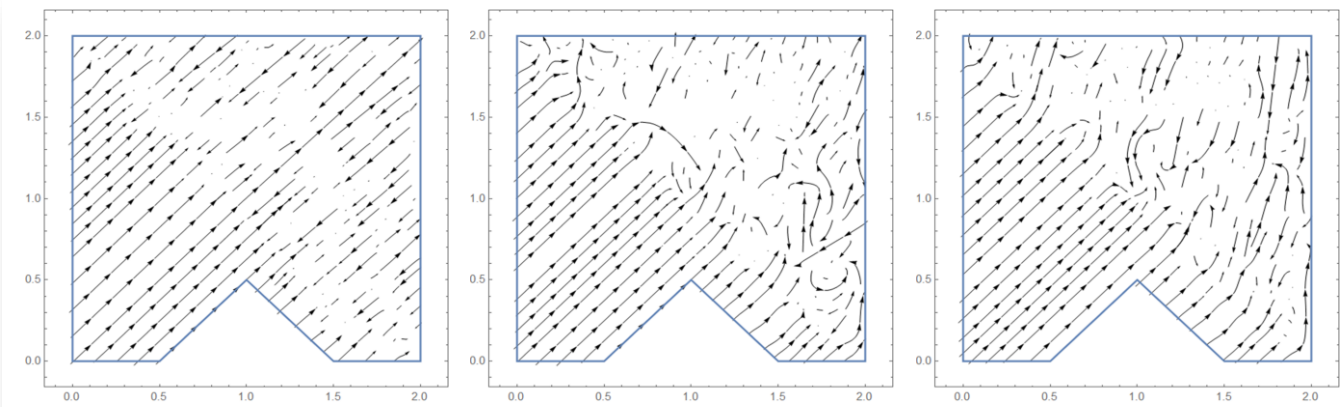

Fig. 13. Stream plots for Q = 15 for different Reynolds numbers: Re = 10, 100 and 5000, respectively.

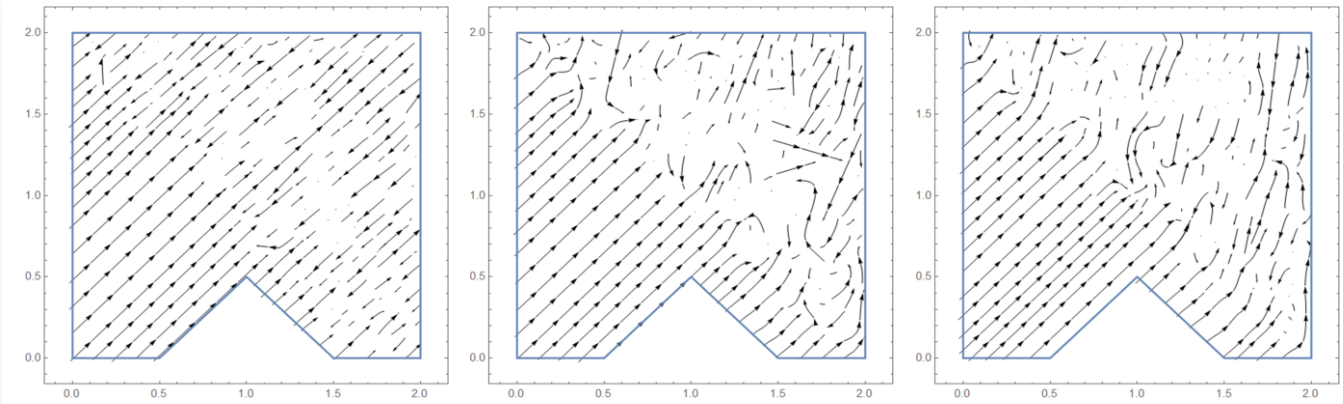

Fig. 14. Stream plots for Q = 24 for different Reynolds numbers: Re = 10, 100 and 5000, respectively.

channel due to the relatively lower heat generation, which causes heat to accumulate near the bottom before it can be adequately dispersed. As the heat source parameter increases, the temperature distribution becomes more uniform, indicating better heat dispersion throughout the channel, suggesting that higher heat source values enhance convective heat transfer, reducing localized temperature peaks. For flows with a higher Reynolds number, the influence of increasing the heat source parameter on the temperature distribution is less pronounced, as higher Reynolds numbers correspond to more turbulent flow regimes that inherently enhance mixing and heat transfer. Thus, even with an increase in Q, the already efficient heat transfer mechanism due to turbulence mitigates significant changes in the temperature distribution.

The combined effect of internal and external heat sources becomes more significant at higher Reynolds numbers, likely due to the enhanced convective heat transfer capabilities in turbulent flows, which can more effectively integrate and distribute

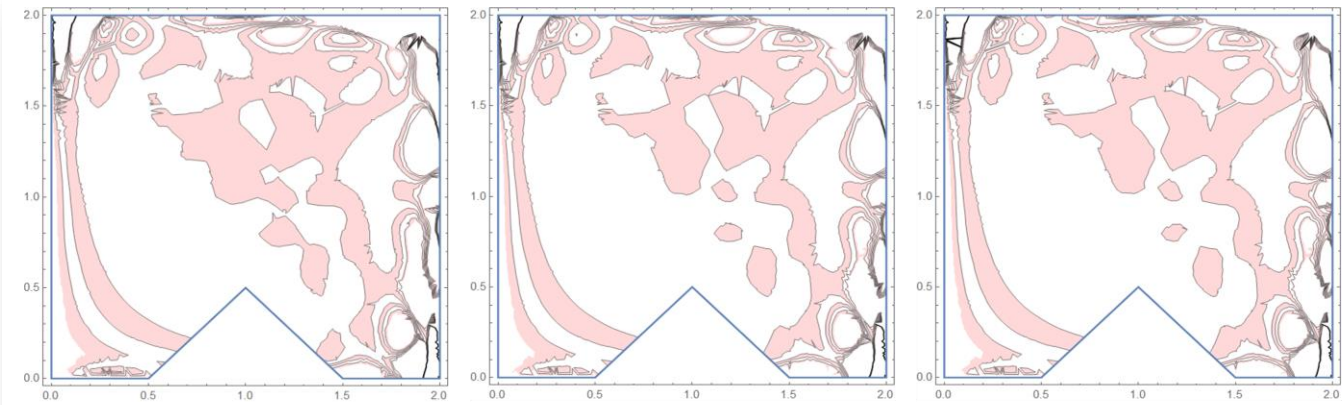

Fig. 15. Contour plots for Q = 5 for different Reynolds numbers: Re = 10, 100 and 5000, respectively.

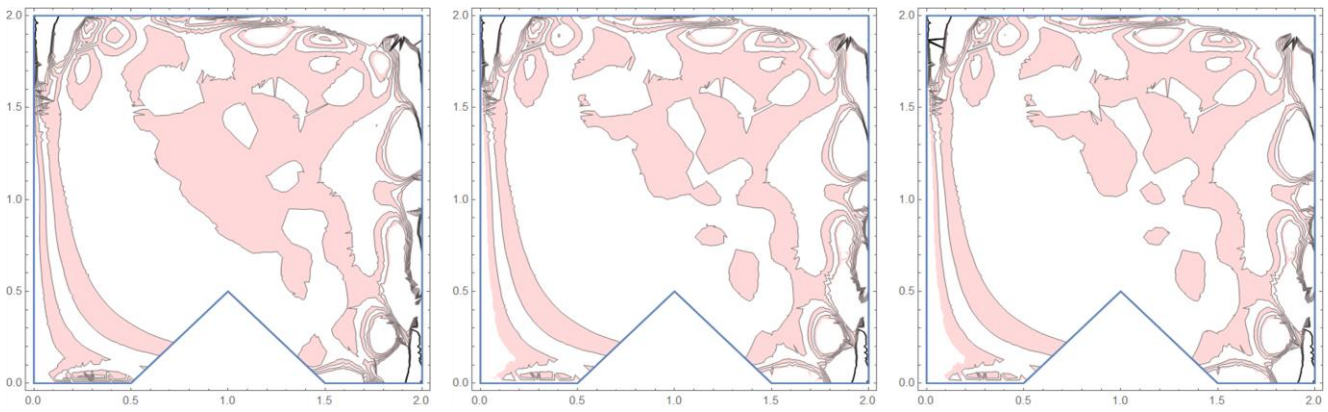

Fig. 16. Contour plots for Q = 12 for different Reynolds numbers: Re = 10, 100 and 5000, respectively.

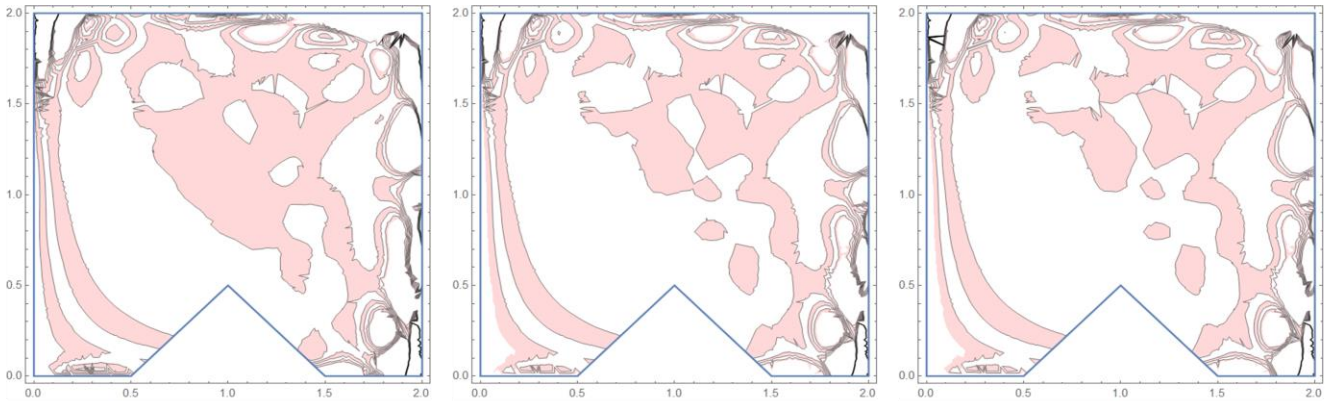

Fig. 17. Contour plots for Q = 15 for different Reynolds numbers: Re = 10, 100 and 5000, respectively.

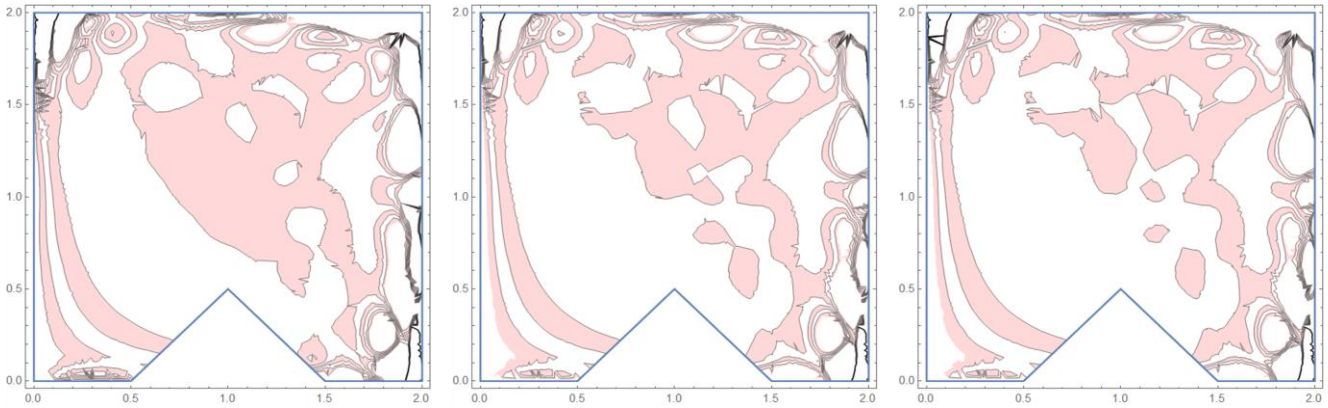

Fig. 18. Contour plots for Q = 24 for different Reynolds numbers: Re = 10, 100 and 5000, respectively.

heat from both sources compared to laminar flows. For all variations of the heat source parameter and Reynolds number, the temperature is consistently higher on the right wall compared to the left wall, possibly due to asymmetries in the flow field or in the placement of heat sources, causing a preferential accumulation of heat on the right side. This observation indicates a potential directional bias in heat transfer within the channel, which may need to be addressed depending on the application or desired thermal management outcomes.

As per Figs. 19–23, the temperature dissemination is larger at high Reynolds numbers for all percentages of CuO particles. This is due to the Brownian motion of CuO particles in the fluid. Further, the thermal boundary layer is found larger near the right wall of the channel than the left wall. The temperature dissemination is found larger near the heat source or bottom of the channel. The dissemination of heat to the top wall is found larger for low Reynolds numbers at all variations of metal particle concentrations.

Figure 24 presents the Nusselt number (Nu), which quantifies the rate of heat transfer across laminar, transitional and turbulent flow regimes. The results indicate that the heat transfer rate increases up to a 3% concentration of metal particles (CuO), beyond which it decreases. This decrease suggests the potential occurrence of particle agglomeration at higher concentrations, impacting heat transfer efficiency. Importantly, this trend is consistent across all Reynolds numbers investigated in this study. For lower Reynolds number flows, the internal heat source significantly boosts heat transfer rates. However, for higher Reynolds numbers, the heat transfer rate shows less predictable behaviour due to the random movement of particles in the fluid, which can disrupt thermal gradients and flow patterns.

The magnetic field parameter (*M*) exhibits varying effects on the heat transfer rate depending on the Reynolds number. In laminar flow, increasing M reduces Nu due to decreased flow induced by the magnetic field. Conversely, at higher Reynolds

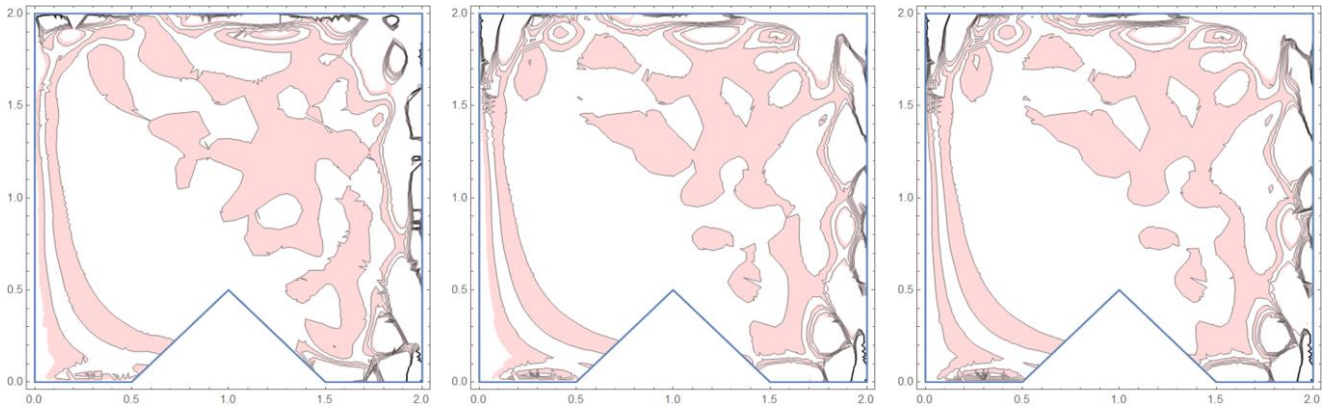

Fig. 19. Contour plots for Ø = 1% for different Reynolds numbers: Re = 10, 100 and 5000, respectively.

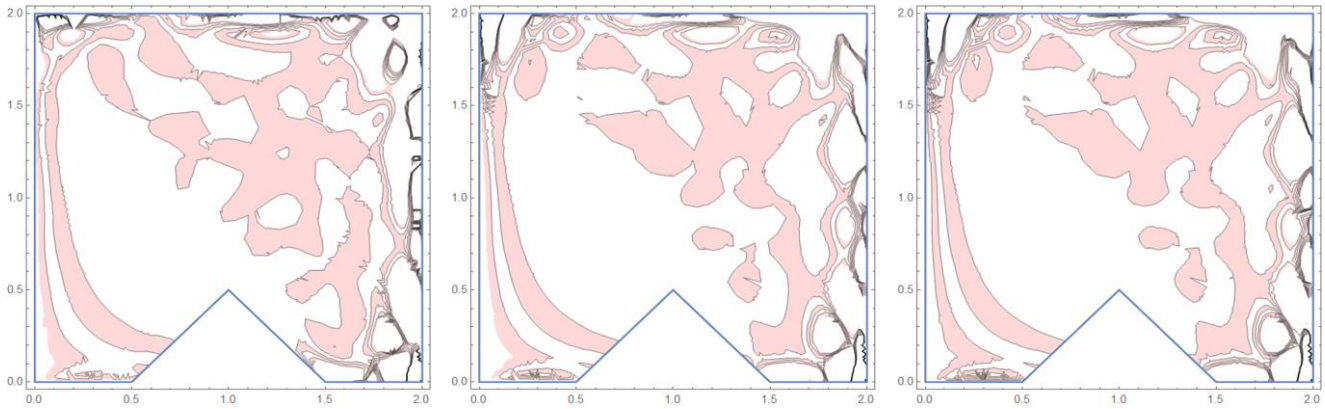

Fig. 20. Contour plots for Ø = 2% for different Reynolds numbers: Re = 10, 100 and 5000, respectively.

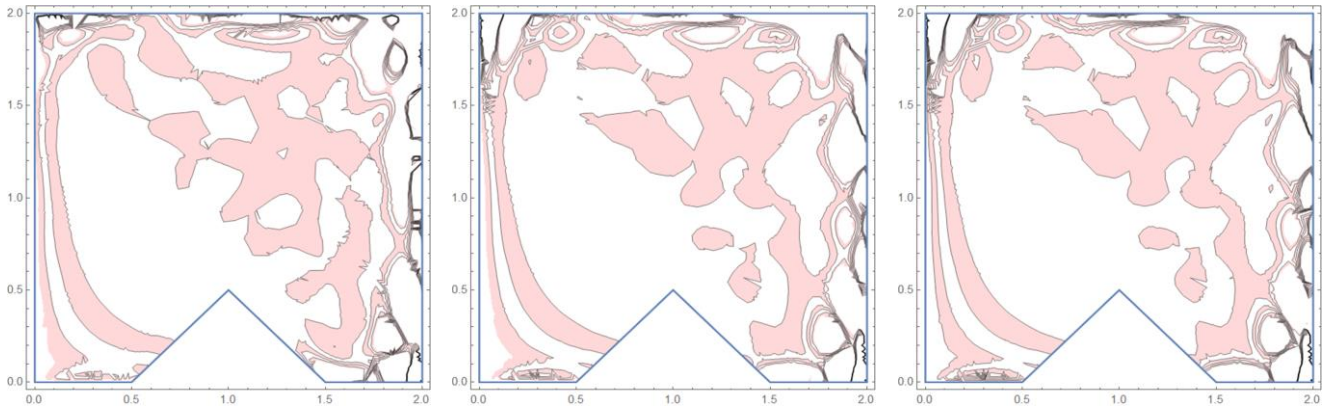

Fig. 21. Contour plots for Ø = 3% for different Reynolds numbers: Re = 10, 100 and 5000, respectively.

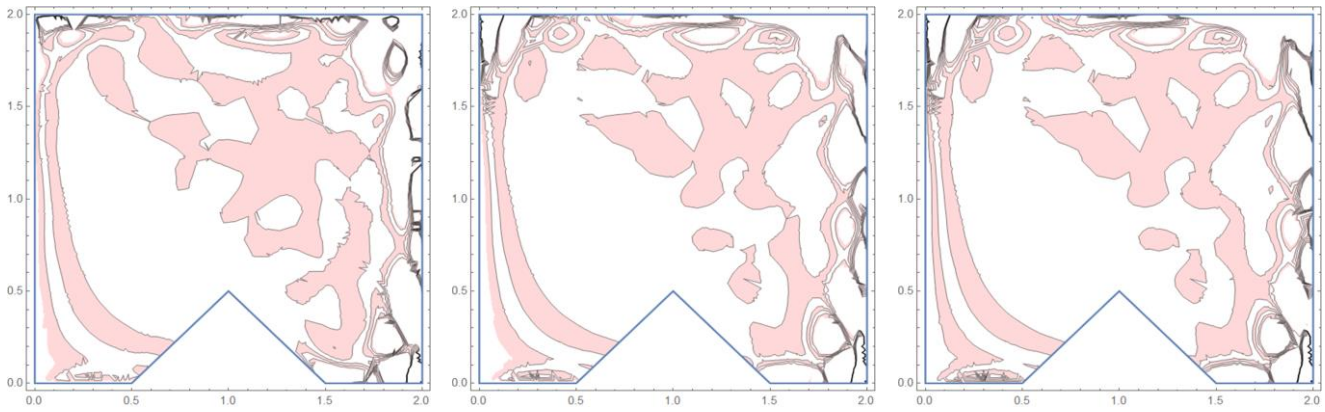

Fig. 22. Contour plots for M = 5 for different Reynolds numbers: Re = 10, 100 and 5000, respectively.

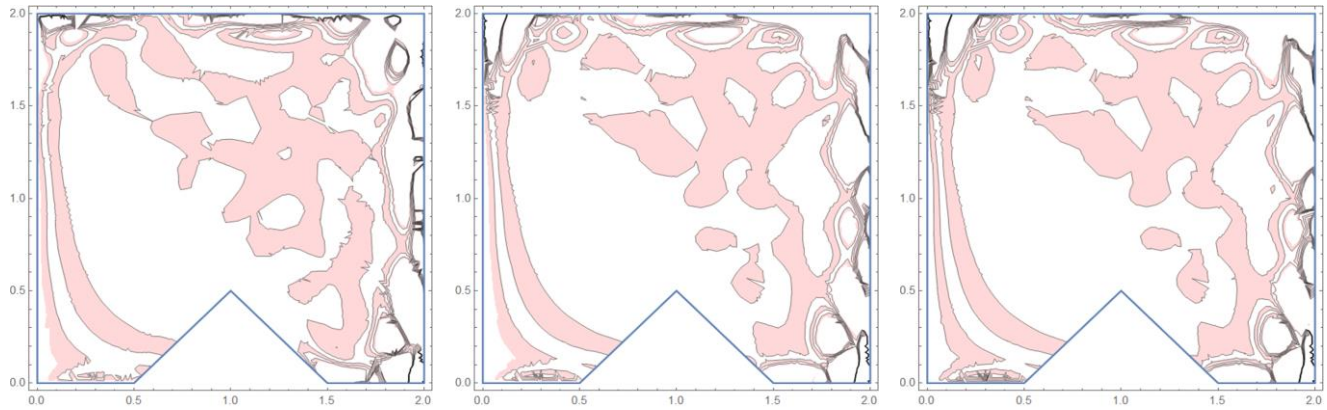

Fig. 23. Contour plots for M = 10 for different Reynolds numbers: Re = 10, 100 and 5000, respectively.

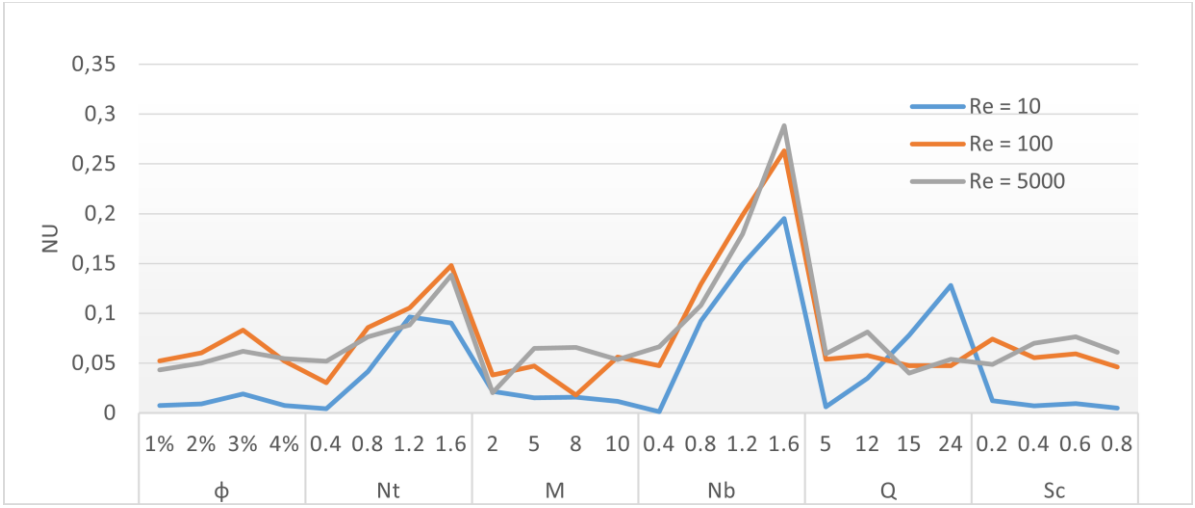

Fig. 24. Nusselt numbers for corresponding variations of parameters.

numbers, the random movement of metal particles may counteract this effect, leading to an increase in Nu with higher M. In summary, Fig. 11 highlights the complex interplay of metal particle centration and magnetic field effects on heat transfer efficiency across different flow conditions. These findings contribute to understanding and optimizing heat transfer processes in nanofluid-based systems under varying operational parameters.

5. Conclusions

The numerical study of flow and heat transfer in CuO-water nanofluid is carried out. The following conclusions are drawn:

1. The stream plots indicate that, at moderate and high Reynolds numbers, the flow in the upper part of the channel significantly weakens, while it remains controlled in the lower part. This behaviour is influenced by the presence of the heat source in the form of a triangular groove. Additionally, the dispersion of CuO metal particles within the fluid contributes to this flow pattern.
2. At higher Reynolds number flows, an increase in the internal heat source typically results in a higher temperature. However, this temperature rise can be mitigated by adjusting the Brownian motion parameter in such flows, especially when Reynolds numbers are high.
3. For effective heat transfer the CuO particle concentration less than 3% is recommended. The magnetic field shows an inconsistent pattern in heat transfer.
4. Limitations: The entire work is limited to heat transfer analysis with the defined geometry. Also, the flow of the fluid is for fixed Reynolds numbers.
5. Future work: This study can be extended to include mass transfer analysis and investigate the impact of additional physical effects, such as variable physical properties, diffusion, or slip conditions. These extensions will provide a more comprehensive understanding of the coupled heat and mass transfer phenomena in the geometry under consideration.

References

[1] Karami, F., Abbasian Arani, A.A., Akbari, O.A., Pourfattah, F., & Toghraie, D. (2023). Numerical study of location and depth of rectangular grooves on the turbulent heat transfer performance and characteristics of CuO-water nanofluid flow. *Heliyon*, 9(3), e14239. doi: 10.1016/j.heliyon.2023.e14239

[2] Dehghani-Ashkezari, E., & Salimpour, M.R. (2018). Effect of groove geometry on pool boiling heat transfer of water-titanium oxide nanofluid. *Heat and Mass Transfer, 54*(11), 3473–3481. doi: 10.1007/s00231-018-2388-1

[3] Boukerma, K., & Kadja, M. (2017). Convective heat transfer of Al2O3 and CuO nanofluids using various mixtures of water-ethylene glycol as base fluids. *Engineering, Technology and Applied Science Research*, 7(2), 1496–1503. doi: 10.48084/etasr.1051

[4] Jafarimoghaddam, A., & Aberoumand, S. (2016). On the implementation of Cu/ethylene glycol nanofluids inside an annular pipe under a constant wall temperature boundary condition. *Heat Transfer−Asian Research*, 46(7), 647–655. doi:10.1002/htj.21235

[5] Gosukonda, S, Gorti, V.P.N.S., Baluguri, S.B., & Sakam, S.R. (2015). Particle spacing and chemical reaction effects on convective heat transfer through a nano-fluid in cylindrical annulus. *Procedia Engineering*, 127, 263–270. doi:10.1016/j.proeng.2015.11.359

[6] Gupta, T., Pandey, A.K., & Kumar, M. (2024). Shape factor and temperature-dependent viscosity analysis for the unsteady flow of magnetic Al_2O_3–TiO_3/$C_2H_6O_2$–H_2O using Legendre wavelet technique. *Pramana*, 98(2), 1–19. doi: 10.1007/s12043-024-02756-9

[7] Balasubramanian, R., & Mukeshkumar, P.C. (2017). Performance of the heat transfer behavior of triethylene glycol (TEG) based CuO and SiN nanofluids in a rectangular pipe under the turbulent flow condition. *Advances in Natural and Applied Sciences*, 11(8), 331–341.

[8] Navaei, A.S., Mohammed, H.A., Munisamy, K.M., Yarmand, H., & Gharehkhani, S. (2015). Heat transfer enhancement of turbulent nanofluid flow over various types of internally corrugated channels. *Powder Technology*, 286, 332–341. doi: 10.1016/j.powtec.2015.06.009

[9] Rimbault, B., Nguyen, C.T., & Galanis, N. (2014). Experimental investigation of CuO–water nanofluid flow and heat transfer inside a microchannel heat sink. *International Journal of Thermal Sciences*, 84, 275–292. doi: 10.1016/j.ijthermalsci.2014.05.025

[10] Ahmed, M.A., Yusoff, M.Z., Ng, K.C., & Shuaib, N.H. (2015). Numerical investigations on the turbulent forced convection of nanofluids flow in a triangular-corrugated channel. *Case Studies in Thermal Engineering*, 6, 212–225. doi: 10.1016/j.csite.2015.10.002

[11] Ekiciler, R. (2021). Effects of novel hybrid nanofluid (TiO_2–Cu/EG) and geometrical parameters of triangular rib mounted in a duct on heat transfer and flow characteristics. *Journal of Thermal Analysis and Calorimetry*, 143(2), 1371–1387. doi: 10.1007/s10973-020-09913-3

[12] Suresh Babu, B., Srinivas, G., & Reddy, B.R.K. (2011). Finite element analysis of free convection flow with MHD micropolar and viscous fluids in a vertical channel with dissipative effects. *Journal of Naval Architecture and Marine Engineering*, 8(1), 59–69. doi: 10.3329/jname.v8i1.5808

[13] Gupta, T., Pandey, A.K., & Kumar, M. (2024). Effect of Thompson and Troian slip on CNT-Fe_3O_4/kerosene oil hybrid nanofluid flow over an exponential stretching sheet with Reynolds viscosity model. *Modern Physics Letters B*, 38(2), 2350209. doi: 10.1142/S0217984923502093

[14] Ahmed, F., Fuad, M., Akter, F., Gugulothu, R., Jilugu, R.K., Alam, S.B., & Kumar, D. (2021). Investigation of entropy and turbulence characteristics of water-based Al2O3, TiO2, and graphene-oxide nanoparticles in a triangular rod array. *Materials Today: Proceedings*, 47(11), 3364–3369. doi: 10.1016/j.matpr.2021.07.160

[15] Vatani, A., & Mohammed, H.A. (2013). Turbulent nanofluid flow over periodic rib-grooved channels. *Engineering Applications of Computational Fluid Mechanics*, 7(3), 369–381. doi: 10.1080/19942060.2013.11015473

[16] Ajeel, R.K., Salim, W.S.I.W., & Hasnan, K. (2018). Thermal and hydraulic characteristics of turbulent nanofluids flow in trapezoidal-corrugated channels: Symmetry and zigzag shaped. *Case Studies in Thermal Engineering*, 12, 620–635. doi: 10.1016/j.csite.2018.09.011

[17] Alipour, H., Bahiraei, M., & Mashayekhi, R. (2017). Influence of T-semi attached rib on turbulent flow and heat transfer parameters of a silver-water nanofluid with different volume fractions in a three-dimensional trapezoidal microchannel. *Physica E: Low-dimensional Systems and Nanostructures*, 88, 60–76. doi: 10.1016/j.physe.2017.01.014

[18] Hussein, A.M., Sharma, K.V., Bakar, R.A., & Kadirgama, K. (2013). The effect of cross-sectional area of tube on friction factor and heat transfer nanofluid turbulent flow. *International Communications in Heat and Mass Transfer*, 47, 49–55. doi: 10.1016/j.icheatmasstransfer.2013.06.004

[19] Naphon, P., & Nakharintr, L. (2015). Turbulent two-phase approach model for the nanofluids heat transfer analysis flowing through the minichannel heat sinks. *International Journal of Heat and Mass Transfer*, 82, 388–395. doi: 10.1016/j.ijheatmasstransfer.2014.11.019

[20] Gosty, V., Srinivas, G., & Babu, B.S. (2024). Numerical investigation of slip effects on heat and mass transfer in a vertical channel with immiscible micropolar and viscous fluids of variable viscosity. *Heat Transfer*, 53(7), 3987–4012. doi: 10.1002/htj.22659

[21] Upreti, H., Das, A., Kumar, P., & Kumar, M. (2023). Exploring the nanoparticle's shape effect on boundary layer flow of hybrid nanofluid over a thin needle with quadratic Boussinesq approximation: Legendre wavelet approach. *Journal of Thermal Analysis and Calorimetry*, 148(22), 12669–12686. doi: 10.1007/s10973-023-12502-9

[22] Avramenko, A.A., Shevchuk, I.V., & Muratov, V.S. (2015). Heat transfer at film condensation of moving vapor with nanoparticles over a flat surface. *International Journal of Heat and Mass Transfer*, 82, 316–324. doi: 10.1016/j.ijheatmasstransfer.2014.11.007

[23] Ajeel, R.K., Salim, W.S.W., & Hasnan, K. (2018). Numerical investigations of flow and heat transfer enhancement in a semicircle zigzag corrugated channel using nanofluids. *International Journal of Heat and Technology*, 36(4), 1292–1303. doi: 10.18280/ijht.360430

[24] Khudheyer, A.F., Hasan, Z., Shuaib, A.N., & Al-Amery, S. (2021). Turbulent heat transfer for internal flow of ethylene glycol-Al2O3 nanofluid in a spiral grooved tube with twisted tape inserts. *Journal of Thermal Engineering*, 7(4), 761–772. doi: 10.18186/thermal.950571

[25] Pourfattah, F., Karami, F., Abbasian Arani, A.A., & Akbari, O.A. (2017). The numerical investigation of angle of attack of inclined rectangular rib on the turbulent heat transfer of Water-Al2O3 nanofluid in a tube. *International Journal of Mechanical Sciences*, 131, 1106–1116. doi: 10.1016/j.ijmecsci.2017.07.002

[26] Sailaja, B., Srinivas, G., Babu, B.S., & Kumar, G.K. (2020). Free and forced convective heat transfer through a nanofluid in two dimensions past moving vertical plate. *South East Asian Journal of Mathematics & Mathematical Sciences*, 16, 1–15. doi: 10.36963/IJTST.2020070302

[27] Akdag, U., Akcay, S., & Demiral, D. (2014). Heat transfer enhancement with laminar pulsating nanofluid flow in a wavy channel. *International Communications in Heat and Mass Transfer*, 59, 17–23. doi: 10.1016/j.icheatmasstransfer.2014.07.016

[28] Uniyal, A., Maheshwari, N., Sharma, P.K., & Raturi, S. (2022). Recent advancements in evacuated tube solar water heaters: A critical review of the integration of phase change materials and nanofluids with ETCs. *Energies*, 15(23), 8999. doi: 10.3390/en15238999

[29] Gosty, V., Srinivas, G., Babu, B.S., Goud, B.S., Hendy, A.S., & Ali, M. R. (2024). Influence of variable viscosity and slip on heat and mass transfer of immiscible fluids in a vertical channel. *Case Studies in Thermal Engineering*, 58, 104368. doi: 10.1016/j.csite.2024.104368

[30] Bhandari, P., Sharma, R., Singh, A., & Yadav, N. (2024). A review on design alteration in microchannel heat sink for augmented thermohydraulic performance. *Ain Shams Engineering Journal*, 15(2), 102417. doi: 10.1016/j.asej.2023.102417

[31] Pak, B.C., & Cho, Y.I. (1998). Hydrodynamic and heat transfer study of dispersed fluids with submicron metallic oxide particles. *Experimental Heat Transfer*, 11(2), 151–170. doi: 10.1080/08916159808946559